

Reconciling quantum trajectories and stationary quantum distributions in single-photon polarization states

Alfredo Luis¹ and Ángel S. Sanz^{2,3}

¹*Departamento de Óptica, Facultad de Ciencias Físicas, Universidad Complutense, 28040 Madrid, Spain*

²*Instituto de Física Fundamental (IFF-CSIC), Serrano 123, 28006 Madrid, Spain*

³*Department of Physics and Astronomy, University College London,
Gower Street, London WC1E 6BT, United Kingdom*

(Dated: July 16, 2018)

The question of the representation of quantum stationary partially polarized waves as random superpositions of different polarization ellipses is addressed. To this end, the Bohmian formulation of quantum mechanics is considered and extended to quantum optical polarization. As is shown, this approach properly combines definite time-evolving trajectories with rigorous stationary quantum distributions via the topology displayed by the associated phase field.

PACS numbers: 42.50.Ct, 42.25.Ja, 03.50.De, 03.65.Ta

I. INTRODUCTION

In most courses, textbooks, and specialized treatises it is common to introduce the polarization of harmonic waves as an ellipse described by the electric field in a real configuration representation [1]. Within this approach, partial polarization thus arises by the rapid and random succession of more or less different polarization states. In more advanced approaches, though, the Stokes parameters and Poincaré sphere are introduced, which allow us to assess the degree of polarization and make use of the powerful tools provided by the SU(2) group. Moreover, the Stokes parameters also enable a simple connection to the quantum regime in terms of their quantum counterparts, namely, the Stokes operators [2].

Once the Stokes parameters are introduced, usually the polarization ellipses are left behind, so that the statistics of the electric field in the polarization plane are abandoned. This is particularly remarkable within the quantum domain, where uncertainty relations imply that no field state can describe a perfect ellipse, just in the same way that no particle can follow a definite trajectory [3–5]. This thus suggests some kind of quantum mismatching between the intuitive ellipse picture and the more powerful Stokes-Poincaré formalism. More specifically, we find quantum states with the maximum degree of polarization, but with their electric-field distribution far from resembling any ellipse, as seen, for example, in Fig. 2 below (for other examples, see also Fig. 1 in Ref. [3] or Fig. 4 in Ref. [4]). Furthermore, the mismatch seems aggravated for quantum stationary states (i.e., states with definite total photon number). In such a case, the electric-field distribution is constant even for states with the maximum degree of polarization, which should correspond to an electric field rapidly describing an elliptical trajectory.

In this work we investigate whether there is still a possibility to keep the most intuitive approach, where partially polarized waves are devised as random superpositions of different polarization ellipses. To this end, the Bohmian formulation of quantum mechanics [6] or, more

properly speaking, its extension to optics [7, 8], seems to be very convenient. This approach properly combines the two ideas that we want to combine: definite trajectories and rigorous quantum distributions. More specifically, here we are going to study the Bohmian trajectories (or optical paths) for a two-dimensional (2D) isotropic harmonic oscillator, which properly represents in the quantum domain a transversal two-mode harmonic wave. For definiteness, and for the sake of simple illustration, we consider single-photon pure states. Accordingly, we have organized this work as follows. In Sec. II we introduce the basic elements involved in the representation of single-photon polarization states. In Sec. III the associated Bohmian dynamics is analyzed and discussed. Finally, in Sec. IV the main conclusions drawn from this work are summarized.

II. POLARIZATION OF ONE-PHOTON STATES

A. Polarization ellipse

Consider a harmonic light wave consisting of two modes of the same frequency, ω , and with their corresponding electric fields vibrating along orthogonal directions. These two modes are represented by their complex amplitude operators \hat{a}_1 and \hat{a}_2 . This system is equivalent to a particle in a 2D isotropic harmonic potential. The equivalence becomes clearer through the quadrature operators representing the real and imaginary parts of the electric field, $\hat{a}_j \propto \hat{X}_j + i\hat{Y}_j$, with

$$\hat{X}_j = \frac{1}{\sqrt{2}} (\hat{a}_j^\dagger + \hat{a}_j), \quad \hat{Y}_j = \frac{i}{\sqrt{2}} (\hat{a}_j^\dagger - \hat{a}_j), \quad (1)$$

and commutator $[\hat{X}_j, \hat{Y}_k] = i\delta_{jk}$, with $j, k = 1, 2$. The \hat{X}_j and \hat{Y}_j operators are thus formally equivalent, respectively, to the (dimensionless) position and momentum of a 2D massive particle. For simplicity, and to exploit as much as possible this equivalence, we assume $\hbar = 1$, $\omega = 1$, and $m = 1$, with the latter being the mass of the

equivalent effective particle. The corresponding effective Hamiltonian then reads as $\hat{\mathcal{H}} = \hat{a}_1^\dagger \hat{a}_1 + \hat{a}_2^\dagger \hat{a}_2$.

The quadrature operators, \hat{X}_j (with $j = 1, 2$), also allow us to introduce a wave function for the 2D real electric field by projection of the field state $|\psi\rangle$ on the unnormalized joint eigenstate of the quadrature operators $\hat{X}_j|x_1, x_2\rangle = x_j|x_1, x_2\rangle$. In particular, for photon-number eigenstates, with $\hat{a}_j^\dagger \hat{a}_j|n_1, n_2\rangle = n_j|n_1, n_2\rangle$, we have

$$\langle x_1, x_2|n_1, n_2\rangle = \mathcal{N}_{12} H_{n_1}(x_1) H_{n_2}(x_2) e^{-(x_1^2 + x_2^2)/2}, \quad (2)$$

where $\mathcal{N}_{12} = (2^{n_1+n_2} \pi n_1! n_2!)^{-1/2}$ is the norm and H_{n_j} are the corresponding Hermite polynomials. Accordingly, the quantum analog of the polarization ellipse is the distribution for the 2D real electric field [3–5],

$$P(x_1, x_2, t) = |\langle x_1, x_2|\psi(t)\rangle|^2, \quad (3)$$

with $|\psi(t)\rangle = \exp(-i\hat{\mathcal{H}}t)|\psi(0)\rangle$.

B. Stokes parameters

Regarding the Stokes picture of polarization, it can be well started from the Stokes operators [2],

$$\begin{aligned} \hat{S}_0 &= \hat{a}_1^\dagger \hat{a}_1 + \hat{a}_2^\dagger \hat{a}_2, \\ \hat{S}_x &= \hat{a}_1^\dagger \hat{a}_1 - \hat{a}_2^\dagger \hat{a}_2, \\ \hat{S}_y &= \hat{a}_2^\dagger \hat{a}_1 + \hat{a}_1^\dagger \hat{a}_2, \\ \hat{S}_z &= i(\hat{a}_2 \hat{a}_1^\dagger - \hat{a}_1 \hat{a}_2^\dagger), \end{aligned} \quad (4)$$

which satisfy the commutation relations

$$[\hat{S}_x, \hat{S}_y] = -2i\hat{S}_z, \quad (5)$$

with cyclic permutations, and

$$\hat{S}^2 = \hat{S}_0(\hat{S}_0 + 2\hat{\mathbb{I}}), \quad [\hat{\mathbf{S}}, \hat{S}_0] = \hat{\mathbf{0}}, \quad (6)$$

with $\hat{\mathbf{S}} = (\hat{S}_x, \hat{S}_y, \hat{S}_z)$. The classical Stokes parameters are the mean values of the Stokes operators, $s_j = \langle \hat{S}_j \rangle$. Because of the non-vanishing commutator, as described by Eq. (5), no state can have definite values of all Stokes operators simultaneously (the only exception being the two-mode vacuum, where they vanish trivially). This is conveniently expressed by the uncertainty relation

$$\begin{aligned} (\Delta \hat{\mathbf{S}})^2 &= (\Delta \hat{S}_x)^2 + (\Delta \hat{S}_y)^2 + (\Delta \hat{S}_z)^2 \\ &= \langle \hat{S}_0(\hat{S}_0 + 2\hat{\mathbb{I}}) \rangle - \langle \hat{\mathbf{S}} \rangle^2 \geq 2\langle \hat{S}_0 \rangle, \end{aligned} \quad (7)$$

which holds after Eq. (6) [9], taking into account that $|\langle \hat{\mathbf{S}} \rangle| \leq \langle \hat{S}_0 \rangle$.

Consider now the standard (classical) definition of the degree of polarization $\mathcal{P} = |\mathbf{s}|/s_0$. Some other more complete definitions, though, have also been proposed, particularly within the quantum domain [4, 5, 10]. Based on the fact that $|\mathbf{s}| \leq s_0$, the Stokes parameters readily provide a representation for polarization states in a

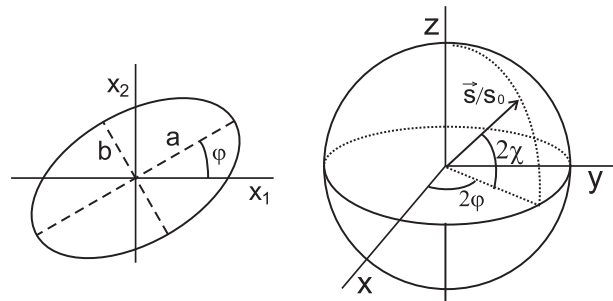


FIG. 1: Polarization ellipse (left) and Poincaré sphere (right).

unit sphere, namely, the Poincaré sphere. This is done through the parametrization

$$\begin{aligned} s_x &= s_0 \cos(2\chi) \cos(2\varphi), \\ s_y &= s_0 \cos(2\chi) \sin(2\varphi), \\ s_z &= s_0 \sin(2\chi), \end{aligned} \quad (8)$$

which is sketched in Fig. 1. In the transformation relations (8), $\tan(2\varphi) = s_y/s_x$, with φ being the angle between the major axis of the polarization ellipse and the x_1 axis. Regarding χ , this angle determines the ratio between the minor and major axes of the polarization ellipse (b and a , respectively), with $\pi/4 \geq \chi \geq -\pi/4$ and $\tan \chi = \pm b/a$, where the sign is given by the handedness (right-handed if $s_z > 0$ and left-handed if $s_z < 0$). The relations (8) thus provide us with a one-to-one correspondence between the Stokes parameters (or points on the Poincaré sphere) and some average or mean polarization ellipse.

C. One-photon states

Let us now consider, more specifically, the most general pure one-photon state. In the photon-number basis $|n_1, n_2\rangle$ it reads as

$$|\psi\rangle = c_1|1, 0\rangle + c_2|0, 1\rangle, \quad (9)$$

with Stokes parameters

$$\begin{aligned} s_0 &= |c_1|^2 + |c_2|^2 = 1, \\ s_x &= |c_1|^2 - |c_2|^2, \\ s_y &= c_1^* c_2 + c_1 c_2^* = 2 \operatorname{Re}(c_1 c_2^*), \\ s_z &= i(c_1^* c_2 - c_1 c_2^*) = 2 \operatorname{Im}(c_1 c_2^*). \end{aligned} \quad (10)$$

These are all stationary states, i.e., $\hat{\mathcal{H}}|\psi\rangle = |\psi\rangle$, so that $|\psi(t)\rangle = \exp(-it)|\psi(0)\rangle$. They are also SU(2) coherent states [11], which are usually considered as classical-like regarding polarization [12], as well as being minimum uncertainty states of the uncertainty relation (7). Moreover, since $|\mathbf{s}| = s_0$ for these states, we have $\mathcal{P} = 1$, thus displaying the maximum degree of polarization according to the classic definition seen above. In spite of this, they cannot be considered as having perfect polarization,

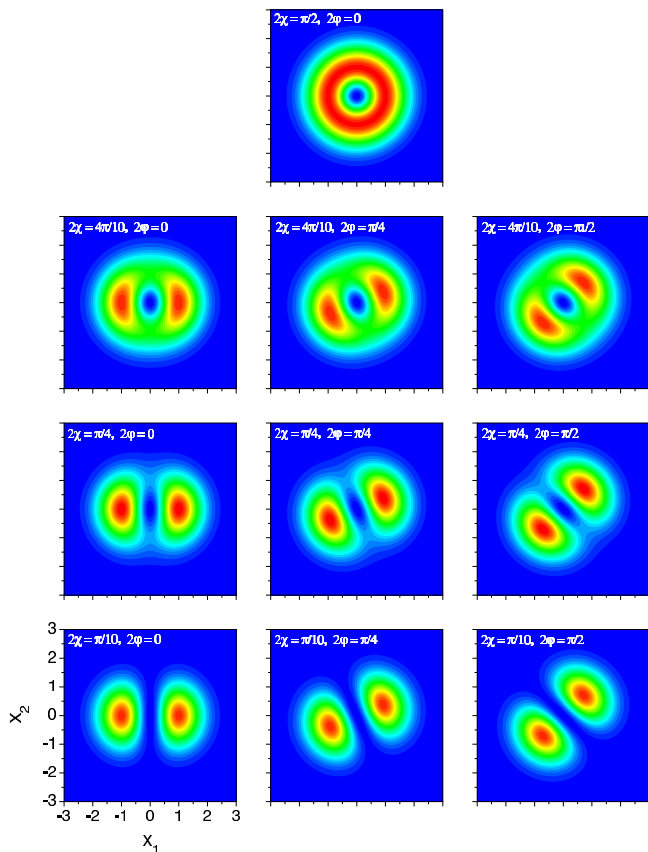


FIG. 2: (Color online) Contour-plots corresponding to the $P(x_1, x_2)$ distribution of the 2D real electric field associated with the pure one-photon state (9). The values chosen for the angles 2χ and 2φ cover the first quadrant of the Poincaré sphere (see Fig. 1, right). Minimum to maximum is indicated with the transition from blue to red, starting from zero in all cases.

since $(\Delta\hat{\mathbf{S}})^2 = 2\langle\hat{S}_0\rangle \neq 0$. This is properly reflected by more complete assessments of the degree of polarization [4, 5, 10].

The quadrature wave function associated with the pure one-photon state (9) is

$$\langle x_1, x_2 | \psi(t) \rangle = \sqrt{\frac{2}{\pi}} (c_1 x_1 + c_2 x_2) e^{-(x_1^2 + x_2^2)/2 - it}, \quad (11)$$

and the corresponding electric-field distribution is

$$P(x_1, x_2) = \frac{1}{\pi} [(1 + s_x)x_1^2 + (1 - s_x)x_2^2 + 2s_y x_1 x_2] e^{-(x_1^2 + x_2^2)} \quad (12)$$

which is effectively independent of time, i.e., it is *stationary*, as expected. In Fig. 2 we show a series of contour-plots of $P(x_1, x_2)$ for angles 2χ and 2φ that cover the first quadrant of the Poincaré sphere; the behavior in the remaining quadrants is analogous and can be inferred by taking into account the corresponding symmetry relations. Also, for convenience regarding the computation of the Bohmian trajectories (see the discussion below),

we have considered the minimum 2χ to be $\pi/10$ instead of 0. As can be seen, only for $2\chi = \pm\pi/2$ and any φ does the picture of an ellipse remain valid (this is for circularly polarized light). As the value of these angles is changed, this picture breaks down despite having the maximum degree of polarization in any of them ($\mathcal{P} = 1$), with the most dramatic breaking off being for $2\chi = 0$, i.e., along the equator of the sphere (this is for linearly polarized light). In this case, $P(x_1, x_2)$ essentially consists of two separate lobes. For $2\varphi = 0$ these lobes are parallel to the x_1 -axis (see the lowest left panel), but their inclination changes as 2φ increases, thus becoming parallel to the x_2 axis when $2\varphi = \pi$ (for the intermediate case, $2\varphi = \pi/2$, they are $\pi/4$ inclined, as seen in the lowest right panel). Apart from deviating from the ellipsoidal picture, it is also worth stressing that information about the handedness will also get lost. This is because $P(x_1, x_2)$ does not depend on s_z .

III. BOHMIAN DYNAMICS

A. Equations of motion

Let us now consider the Bohmian approach with the purpose of grasping some physical insight from the dynamical state associated with the wave function (11). Within this context, the corresponding Bohmian trajectories $\mathbf{r}(t) = [x_1(t), x_2(t)]$ are obtained after integration of the guidance equation

$$\dot{\mathbf{r}} = \nabla S = -ie^{-iS} \nabla e^{iS}, \quad (13)$$

where S is the (real-valued) phase of the wave function (11), i.e.,

$$e^{iS} = \frac{(c_1 x_1 + c_2 x_2) e^{-it}}{\sqrt{|c_1|^2 x_1^2 + |c_2|^2 x_2^2 + (c_1 c_2^* + c_1^* c_2) x_1 x_2}}. \quad (14)$$

In terms of the Stokes parameters, this expression can also be recast as

$$e^{iS} = \frac{\sqrt{1 + s_x} \left[x_1 + \left(\frac{1 - s_x}{s_y + i s_z} \right) x_2 \right] e^{-it + i\delta}}{\sqrt{x_1^2 + x_2^2 + s_x(x_1^2 - x_2^2) + 2s_y x_1 x_2}}, \quad (15)$$

where δ is a global relative phase associated with the coefficient c_1 . This phase factor is physically meaningless regarding the topology displayed by the phase field, S , as well as the trajectory dynamics described by the equation of motion below, as also happens with t . Substituting this expression into Eq. (13), we find

$$\dot{\mathbf{r}} = \frac{s_z}{x_1^2 + x_2^2 + s_x(x_1^2 - x_2^2) + 2s_y x_1 x_2} (x_2, -x_1). \quad (16)$$

In general, Eq. (16) has to be numerically integrated in order to obtain the corresponding trajectories, as seen in Sec. III C below. However, as shown in the next section, it is also possible to draw a series of interesting conclusions directly from the form of Eq. (16), without the need to integrate it.

B. Properties of the trajectories

1. Circular trajectories

In spite of the complex dependence on x_1 and x_2 displayed by the prefactor of the equation of motion (16), the trajectories for any single-photon state with $s_z \neq 0$ are always circular. This comes from the fact that

$$\mathbf{r} \cdot \nabla S = \mathbf{r} \cdot \dot{\mathbf{r}} = 0, \quad (17)$$

which implies that r^2 (and therefore \mathbf{r}) is constant.

Now, for $s_z = 0$, when the photons are linearly polarized, we have $\dot{\mathbf{r}} \equiv \mathbf{0}$ and therefore the whole vector \mathbf{r} will be constant. That is, each separate \mathbf{r} -component is constant with time, since Eq. (17) ensures the time independence only of $r = |\mathbf{r}|$, but not its components (see below). This case can be then regarded as the limit of a circle described at a vanishing speed.

2. Nonuniform angular frequency

The angular frequency of these circular trajectories is not uniform. This is readily seen if we use polar coordinates,

$$x_1 = r \cos \phi, \quad x_2 = r \sin \phi, \quad (18)$$

and then express (16) in terms of these coordinates, which renders the following equation of motion for the polar component:

$$\begin{aligned} \dot{\phi} &= -\frac{s_z/r^2}{1 + s_x \cos 2\phi + s_y \sin 2\phi} \\ &= -\frac{\sin(2\chi)/r^2}{1 + \cos(2\chi) \cos(2\phi - 2\varphi)}. \end{aligned} \quad (19)$$

We recall that the polarization ellipse is described at constant angular speed ω (in our case $\omega = 1$). However, as seen through (19), this is not the case for the Bohmian trajectories, where $\dot{\phi}$ strongly depends on the polarization state (see below). Thus, the only case with uniform angular velocity holds for $\chi = \pm\pi/4$, i. e., for circularly polarized light.

3. Handedness

The handedness of the Bohmian trajectories is the same as for the corresponding polarization ellipses. After the change of coordinates (18), the Bohmian motion will be right-handed if $\dot{\phi} < 0$, while the polarization ellipse is right-handed when $s_z > 0$.

4. Extreme instantaneous frequencies

and ellipse parameters

The maximum instantaneous angular frequency of the Bohmian trajectories, denoted by $\Omega = |\dot{\phi}|$, is

$$\Omega_{\max} = \frac{1}{r^2 |\tan \chi|}, \quad (20)$$

which holds when $\cos(2\phi - 2\varphi) = -1$, i.e., when $\phi = \varphi \pm \pi/2$, modulo π . In other words, this condition is equivalent to saying that the maximum instantaneous angular frequency of the Bohmian trajectory coincides with the direction of the minor axis of the polarization ellipse (see Fig. 1).

On the contrary, the minimum instantaneous angular frequency is

$$\Omega_{\min} = \frac{|\tan \chi|}{r^2}, \quad (21)$$

which holds when $\cos(2\phi - 2\varphi) = 1$, i.e., when $\phi = \varphi$, modulo π . That is, the minimum instantaneous angular frequency coincides with the direction of the major axis of the polarization ellipse. Note, therefore, that the ratio between minimum and maximum instantaneous angular frequencies is

$$\frac{\Omega_{\min}}{\Omega_{\max}} = \tan^2 \chi = \frac{b^2}{a^2}, \quad (22)$$

which coincides with the ratio of the minimum to maximum axes of the polarization ellipse, b and a , respectively.

5. Compatibility with classical electrodynamics and nonclassicality

We recall that the variables x_1 and x_2 are two orthogonal electric-field components, so that the associated $x_1(t)$ and $x_2(t)$ Bohmian trajectories represent the dynamical evolution of the electric field. These orbits are *not* compatible with the Maxwell equations, which demand that the electric field describes an ellipse at constant angular frequency ω (in our case $\omega = 1$). The discrepancy between Bohmian orbits and classical electromagnetism is apparent through Eq. (16). This equation, which expresses the time derivative of the electric field vector, is strongly nonlinear. This is also clearly displayed in Figs. 3, 4, and 5 below, where the jumping behavior of the angular frequencies $\dot{\phi}$ are irreconcilable with the harmonic behavior of classical polarization ellipses.

We find this lack of compatibility with classical electrodynamics very suggestive, since it may be naturally ascribed to the nonclassical nature of stationary one-photon field states (9). Of course, it can be readily shown that for non stationary, classical-like Glauber coherent states the Bohmian orbits are actually ellipses described at constant angular frequency ω , in full agreement with

classical optics. However, the mechanism that generates the dynamics in this case is very different from the one involved in stationary single-photon states. In the case of coherent states the dynamics appears because the phase of the corresponding wave function is time dependent, while in the latter it is just a purely topological property associated with phase-local (time-independent) space variations. In this regard, notice that the rich and nontrivial dynamics displayed by the one-photon orbits is needed to reconcile electric-field dynamics with the counterintuitive stationary electric-field probability distribution associated with nonclassical photon-number light states. This may provide a different perspective on the quantum nature of light states.

C. Numerical simulations

A priori, the properties discussed above may seem counterintuitive and puzzling. For example, how is it possible that the trajectories describe circles if their angular frequency is variable with time, or if they tend to distribute in regions where $P(x_1, x_2)$ is maximum, avoiding the nodal ones? Actually, it seems that there is a mismatching between the symmetry of the wave function and the features characterizing the trajectories. In order to elucidate these questions as well as to reconcile two antagonists, namely, motion and stationarity in the case of single-photon states accounted for by wave functions like (9), we have numerically integrated the equation of motion (16) for some of the conditions considered in Fig. 2. Each condition represents a different single-photon state vector and, therefore, a particular dynamics. The corresponding trajectories as well as some other additional representations of interest are displayed in Figs. 3, 4, and 5. For clarity, the initial condition, $x_1(0) = 1$ and $x_2(0) = 0$, was chosen to be the same in the three cases. Accordingly, all the trajectories will be circles of unit radius and, in principle, indistinguishable, in agreement with (17). Disambiguation follows, though, when one analyzes the time dependence of each component separately or their respective velocities, as can be seen in the additional representations (see also the discussions below). For completeness, and also to verify our conclusions in other cases, we also considered the same cases, but with other radii. The corresponding trajectories will not be plotted here, although we would like to stress the fact that we could corroborate that, effectively, the smaller the radius, the faster the motion around the circle, in agreement with the r^{-2} factor in Eq. (19). Moreover, it has also been noticed that the time needed for trajectories with the same radius to complete the circle is different, increasing as 2χ approaches zero. This can be seen below by examining the dependence on time of the velocity components of the trajectories, i.e., $v_i = \dot{x}_i$, with $i = 1, 2$ [see the red dashed line in panels (c) and (d) of Figs. 3, 4, and 5]. Thus, as 2χ approaches zero, one observes a certain bistable behavior: v_1 and v_2

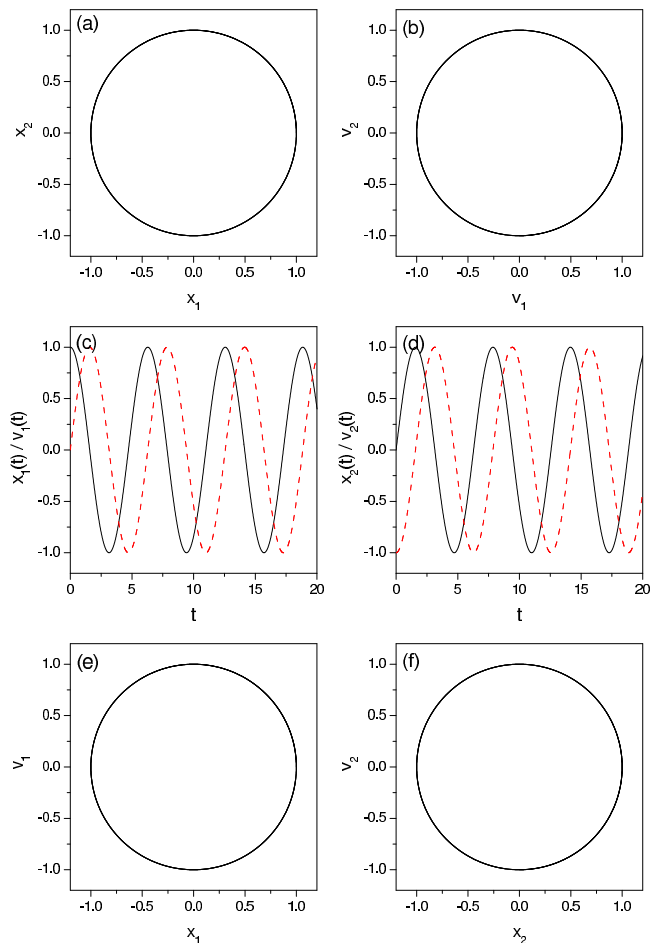


FIG. 3: (Color online) Different representations of the Bohmian trajectories associated with a single-photon polarization state characterized by $2\chi = \pi/2$ and $2\varphi = 0$ on the Poincaré sphere. In (c) and (d) the black solid lines denote the spatial component (x_1 or x_2), while the red dashed line refers to the respective velocity component (v_1 or v_2). In the corresponding panels, the velocity components have been obtained by evaluating (16) along the trajectory.

undergo important variations in extremely short periods of time, while they remain finite (or even vanishing) for relatively long times, thus conferring a certain stationarity or stability to the corresponding photon state. This fact is actually in correspondence with the last of the properties studied in Sec. III B.

Going now to each particular case, in Fig. 3 we have displayed the results for circularly polarized light $2\chi = \pi/2$ and $2\varphi = 0$ on the Poincaré sphere (see Fig. 1). Notice that the evolution is ruled by a harmonic motion. This can be seen through the time dependence of the components x_1 and x_2 , and their corresponding velocities v_1 and v_2 [see Figs. 3(c) and 3(d)], or through the respective phase-space orbits [see Figs. 3(e) and 3(f)]. In this case, $s_z = s_0 = 1$ and $s_x = s_y = 0$, which means that the photon has equal probability to be in the $|1, 0\rangle$

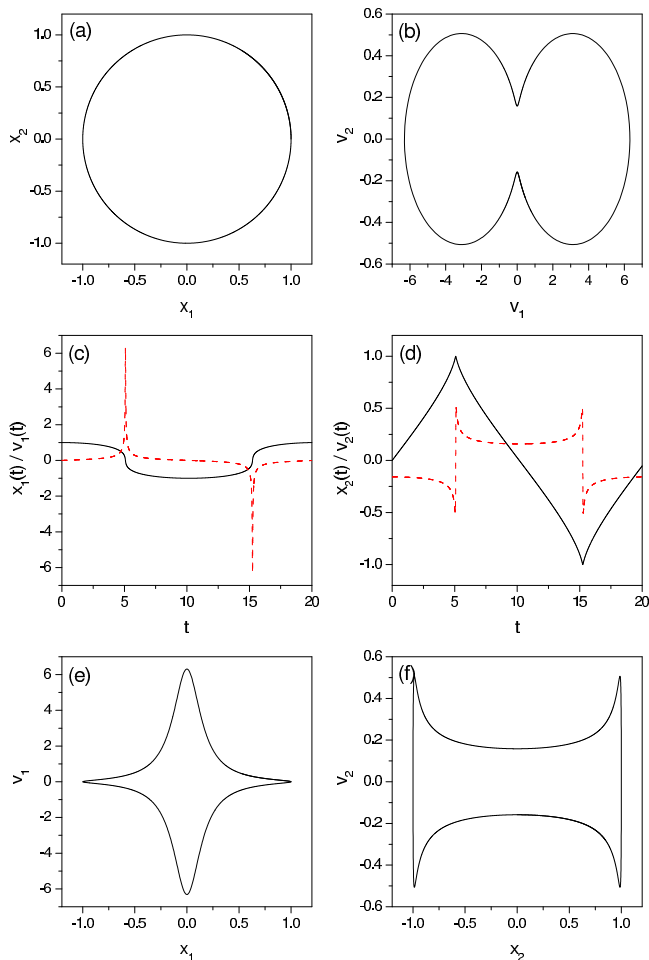


FIG. 4: (Color online) As in Fig. 3, but for $2\chi = \pi/10$ and $2\varphi = 0$.

state as in the $|0, 1\rangle$ state. Therefore, this uncertainty leads the trajectory to visit all points on a circle of a given radius at the same (angular) velocity, this eventually manifesting as a harmonic-like motion or oscillation between $|1, 0\rangle$ and $|0, 1\rangle$ (or, in other terms, between the horizontal and vertical polarization states).

As we move towards the equator of the Poincaré sphere, i.e., vanishing s_z for linearly polarized light (from top to bottom in Fig. 2), the torus-like distribution starts developing two lobes, which in the limit $s_z = 0$ become separate. Here we find an apparently paradoxical behavior: $P(x_1, x_2)$ consists of two separate lobes, but the trajectories are still circles, as indicated by (17). To analyze this situation, we have proceeded as before, but considering the single-photon state defined by $2\chi = \pi/10$ and $2\varphi = 0$ (see Fig. 4). In order to reconcile both behaviors, principally because no trajectory should be expected at a nodal region (these are regions of lowest probability), it is important to observe the time dependence of x_1 and x_2 , displayed in Figs. 4(c) and 4(d), respectively. In the case of x_1 , we note a bistable behavior. That is, x_1 is

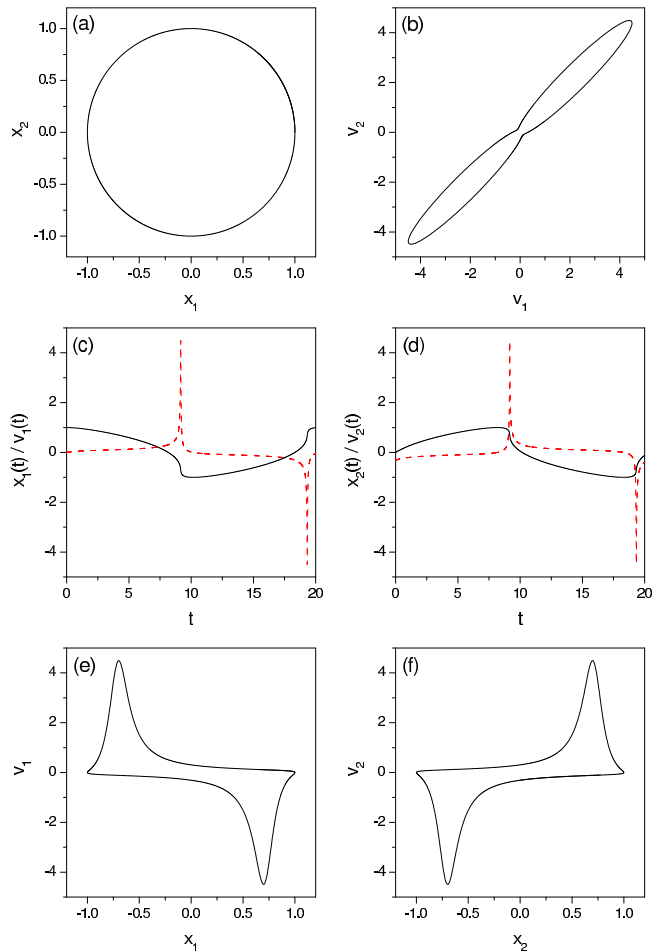


FIG. 5: (Color online) As in Fig. 3, but for $2\chi = \pi/10$ and $2\varphi = \pi/2$.

essentially $+1$ or -1 for relatively long periods of time (which are expected to increase as $2\chi \rightarrow 0$), while x_2 only oscillates linearly, up-and-down, between these values to compensate the transition from x_1 to x_2 . We observe that such transitions are extremely fast. Actually, in the case of x_1 , the velocity v_1 is negligible except at the transition times, while v_2 fluctuates between two almost stationary values ($+0.16$ and -0.16 , approximately). As a consequence, the system will remain apparently either in one lobe or the other of $P(x_1, x_2)$, as shown by the orbit of the velocity representation displayed in Fig. 4(b) (if we consider $2\varphi \rightarrow \pi$, we will find the same, but replacing x_1 by x_2 , and vice versa).

The situation is similar if we move around the equatorial plane regarding the presence of the two lobes in $P(x_1, x_2)$, although this motion implies a rotation of the axis along which they are distributed. As mentioned in Sec. II C, the lobes are aligned with the x_1 axis for $2\varphi = 0$ and start inclining counterclockwise as this angle increases, becoming aligned with the x_2 axis when $2\varphi = \pi$. This change affects not only the distribution $P(x_1, x_2)$, but also the phase of the single-photon state

and therefore its associated trajectory dynamics. To illustrate this case, we are going to consider the state described by $2\chi = \pi/10$ and $2\varphi = \pi/2$ (see Fig. 5), which is linked to the distribution displayed in the lowest right panel of Fig. 2. Although the trajectory is still circular, the orbit in the velocity space describes two lobes distributed along a $\pi/4$ axis [see Fig. 5(b)], which in the limit $2\chi \rightarrow 0$ will end up in a line with a $\pi/4$ inclination. Note that these lobes constitute a distortion of those displayed by the velocities in the previous case [compared with Fig. 4(b)]. In Figs. 5(c) and 5(d) we observe that this behavior just means that the photon oscillates between one lobe of the distribution $P(x_1, x_2)$ and the other in a rather inhomogeneous way: there is a slow, gradual approach to the transition followed by a sudden switch, as indicated by the corresponding velocities. In the corresponding phase-spaces [see Figs. 5(e) and 5(f)], we observe precisely that the velocity reaches its maximum value right after the photon has reached one of the lobes [of $P(x_1, x_2)$] and just before it jumps into the other. Nonetheless, although the angular velocity is rather nonuniform, the trajectory is still circular.

Finally, we would like to illustrate the source of motion in the kind of stationary state considered here. In contrast to non-stationary wave functions, where the time-dependence of the phase leads naturally to time-evolving trajectories [13, 14], here motion has a topological origin: the space-dependent (configuration space) gradient of the global phase associated with the stationary state. In Fig. 6 we show the distribution $P(x_1, x_2)$ (upper row), the phase S (second row), and the components of the local velocity field, v_1 and v_2 (in the third and fourth rows, respectively), of the three cases represented in Figs. 3, 4, and 5 (left, central, and right columns, respectively). From a quick inspection, the role of the phase-field topology on the trajectory dynamics becomes readily apparent. This field decreases monotonically counterclockwise, thus explaining the evolution of the trajectories (from their beginning, as x_1 decreases, x_2 increases). Now, while this decrease is gradual for $2\chi = \pi/2$, it becomes step-like as 2χ approaches zero. In the latter case, the step lies precisely along the symmetry axis passing between the two lobes. In this sense, the motion is relatively slow along each plateau of the phase field and very fast when the trajectory comes down the step (i.e., passes from the region covered by one of the lobes to the region covered by the other). This has a straightforward counterpart in the corresponding velocity field components. For $2\chi = 0$ these components are symmetric with respect to a $\pi/2$ rotation, which is a signature of harmonic motion (as one of the components starts to decrease, the other increases, and vice versa). Now, as 2χ approaches zero we find two types of behaviors. For $2\chi = 0$ and $2\varphi = 0$, the component along the step of the phase field becomes more prominent than the component that is perpendicular to this step, which eventually becomes meaningless. This is in correspondence with the fact that it is more likely to find the trajectory either in

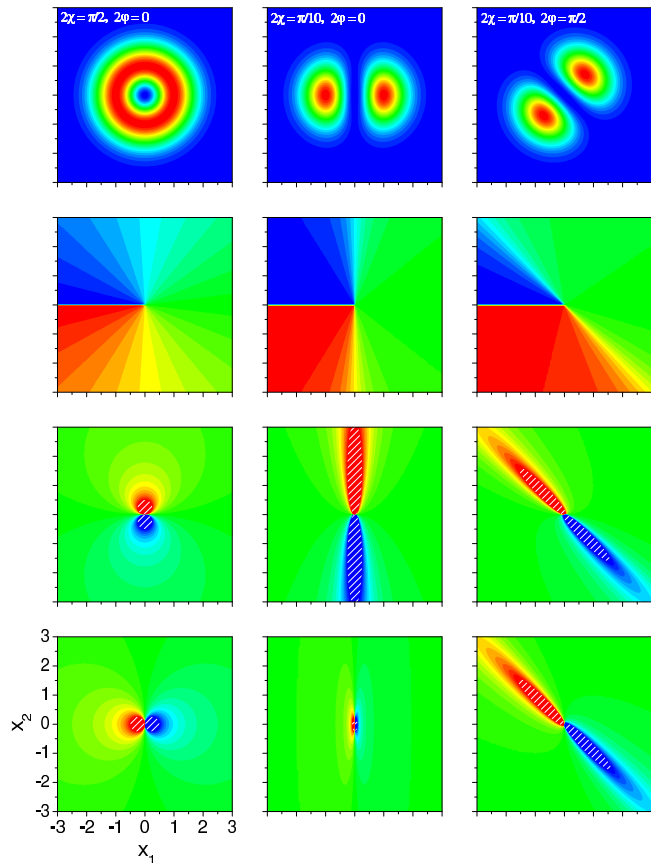


FIG. 6: (Color online) Distribution $P(x_1, x_2)$ (top row), phase field S (second row), and components of the local velocity field, v_1 and v_2 (third and fourth rows, respectively), for the polarization states considered in Figs. 3, 4, and 5 (left, central, and right columns, respectively). Minimum to maximum is indicated with the transition from blue to red: for $P(x_1, x_2)$, starting from zero in all cases; for S , between $-\pi$ and $+\pi$; and for v_1 and v_2 , between -2 and $+2$. In the last two rows the shaded areas indicate a truncation to the maximum and minimum values chosen.

the right or the left lobe of $P(x_1, x_2)$ (small v_1 and v_2), but not in between (large v_1). A similar behavior, but exchanging the axes, would be found for $2\chi = 0$ with $2\varphi = \pi$. Now, as 2φ moves towards $\pi/2$, the two components tend to align, thus becoming equal for $2\varphi = \pi/2$, which means that the trajectories will avoid staying in the neighborhood of the diagonal $x_2 = -x_1$.

IV. CONCLUSIONS

In this work we have shown that the topology displayed by the Bohmian trajectories analyzed has no relation whatsoever with the form of the polarization ellipse of the corresponding field state, since they are always circles. However, the angular speed at which these circles are described contains complete information about the

mean polarization state, i.e., the ellipse traditionally associated with the Stokes parameters. This information is paradoxically absent from the probability distribution corresponding to the 2D real electric field [see Eq. (12)], where one would expect to see the quantum counterpart of the classical mean ellipse. Moreover, seemingly, the Bohmian trajectories provide no hint about the uncertainty of the polarization state, since the families of trajectories associated with a given field state are essentially identical.

Concerning the dynamics associated with single-photon polarization states, we have found a relatively rich variety of behaviors depending on the point on the Poincaré sphere defining the state vector. As seen, although all the trajectories are circles, their dynamical evolution is strongly dependent on their position with respect to the Poincaré sphere, ranging thus from harmonic behaviors (for trajectories on the poles) to bistable oscillating ones (for trajectories on the equator). In all cases, though, this dynamics has a clear topological origin associated with the particular shape of the phase field, which goes from a gradual decrease around $(x_1, x_2) = (0, 0)$ (at the poles) to a step-like one (on the equator). Accordingly, trajectories evolve counterclockwise either harmonically or displaying jumps, respectively.

The fact that polarization stationary states may have an associated internal or intrinsic dynamics is puzzling as well as challenging, for it goes beyond our physical intuition even if it is proven mathematically, as was done here. Even though distributions like $P(x_1, x_2)$ are invariant objects with time, there is a dynamics induced by the phase-field topology. This poses the interesting and stimulating question of whether such an intrinsic motion could be experimentally measured. Note that recently

Steinberg and co-workers were able to experimentally infer [15] the Bohmian trajectories or averaged photon paths [7] in a two-slit experiment by means of weak measurements [16, 17]. The ideas posed here clearly point towards a further extension of this work in this direction with the ultimate goal of performing such experimental measurements. This would allow us to better understand the nature of stationary states as situations where the system is statistically described by a time-independent (steady) distribution, but that display particular inner dynamics. Obviously, this has a potential interest in quantum information and quantum computation, where the basic ingredient, the qubit, is precisely described by a state like (9). Furthermore, also notice the implication in quantum mechanics, where the role equivalent to polarization is played by the particle spin. This vectorial quantity is traditionally assigned to an internal rotation, because it fulfils the same properties of the rotation group. With the picture on stationary states provided above, based on a dynamical grounds, this connection becomes even clearer.

Acknowledgments

Support from the Ministerio de Economía y Competitividad (Spain) under Projects No. FIS2012-35583 (A.L.), No. FIS2010-22082 (A.S.), and No. FIS2011-29596-C02-01 (A.S.), and a “Ramón y Cajal” Grant (A.S.); from the Consejería de Educación de la Comunidad de Madrid under Project No. QUITEMAD S2009-ESP-1594 (A.L.); and from the COST Action MP1006 “Fundamental Problems in Quantum Physics” (A.S.) is acknowledged. A.S. also thanks the University College London for its kind hospitality.

-
- [1] M. Born and E. Wolf, *Principles of Optics*, 7th expanded ed. (Cambridge University Press, Cambridge, England, 1999); Ch. Brosseau, *Fundamentals of Polarized Light: A Statistical Optics Approach* (Wiley, New York, 1998).
 - [2] J. Schwinger, *Quantum Theory of Angular Momentum*, (Academic Press, New York, 1965).
 - [3] J. Pollet, O. Méplan, and C. Gignoux, *J. Phys. A* **28**, 7287 (1995).
 - [4] A. Luis, *Phys. Rev. A* **66**, 013806 (2002).
 - [5] J. Liñares, M. C. Nistal, D. Barral, and V. Moreno, *Eur. J. Phys.* **31**, 991 (2010); J. Liñares, D. Barral, M. C. Nistal, and V. Moreno, *J. Mod. Opt.* **58**, 711 (2011).
 - [6] D. Bohm, *Phys. Rev.* **85**, 166 (1952); **85**, 180 (1952); P. R. Holland, *The Quantum Theory of Motion* (Cambridge University Press, Cambridge, England, 1993); A. S. Sanz and S. Miret-Artes, *Am. J. Phys.* **80**, 525 (2012); X. Oriols and J. Mompart, *Overview of Bohmian Mechanics, in Applied Bohmian Mechanics: From Nanoscale Systems to Cosmology*, edited by X. Oriols and J. Mompart (Pan Stanford Publishing, Singapore, 2012), Chap. 1, pp. 15–147.
 - [7] A. S. Sanz, M. Davidović, M. Božić, and S. Miret-Artés, *Ann. Phys. (N.Y.)* **325**, 763 (2010).
 - [8] A. S. Sanz, J. Campos-Martínez, and S. Miret-Artés, *J. Opt. Soc. Am. A* **29**, 695 (2012).
 - [9] R. Delbourgo, *J. Phys. A* **10**, 1837 (1977).
 - [10] A. Picozzi, *Opt. Lett.* **29**, 1653 (2004); Ph. Réfrégier, *ibid.* **30**, 1090 (2005); A. B. Klimov, L. L. Sánchez-Soto, E. C. Yustas, J. Söderholm, and G. Björk, *Phys. Rev. A* **72**, 033813 (2005); Ph. Réfrégier and F. Goudail, *J. Opt. Soc. Am. A* **23**, 671 (2006); L. L. Sánchez-Soto, J. Söderholm, E. C. Yustas, A. B. Klimov, and G. Björk, *J. Phys.: Conf. Ser.* **36**, 177 (2006); I. Ghiu, G. Björk, P. Marian, and T. A. Marian, *Phys. Rev. A* **82**, 023803 (2010).
 - [11] F. T. Arecchi, E. Courtens, R. Gilmore, and H. Thomas, *Phys. Rev. A* **6**, 2211 (1972).
 - [12] O. Giraud, P. Braun, and D. Braun, *Phys. Rev. A* **78**, 042112 (2008).
 - [13] A. S. Sanz and S. Miret-Artes, *Chem. Phys. Lett.* **445**, 350 (2007).
 - [14] A. S. Sanz and S. Miret-Artes, *J. Phys. A* **41**, 435303 (2008).
 - [15] S. Kocsis, B. Braverman, S. Ravets, M. J. Stevens, R. P.

- Mirin, L. K. Shalm, and A. M. Steinberg, *Science* **332**, 1170 (2011).
- [16] Y. Aharonov and L. Vaidman, *Phys. Rev. A* **41**, 11 (1990).
- [17] B. Hiley, *J. Phys.: Conf. Ser.* **361**, 012014 (2012).